IEEE Access
Multidisciplinary | Rapid Review | Open Access Journal

Received May 12, 2020, accepted June 1, 2020, date of publication June 4, 2020, date of current version June 18, 2020.

Digital Object Identifier 10.1109/ACCESS.2020.3000134

Eight-Port Metamaterial Loaded UWB-MIMO Antenna System for 3D System-in-Package Applications

TAYYAB SHABBIR[1], RASHID SALEEM[2], SAMIR SALEM AL-BAWRI[3,4], (Member, IEEE), MUHAMMAD FARHAN SHAFIQUE[5], (Senior Member, IEEE), AND MOHAMMAD TARIQUL ISLAM[1], (Senior Member, IEEE)

[1]Department of Electrical, Electronic and Systems Engineering, Faculty of Engineering and Built Environment, Universiti Kebangsaan Malaysia, Bangi 43600, Malaysia
[2]Department of Telecommunication Engineering, University of Engineering and Technology, Taxila 47050, Pakistan
[3]Faculty of Engineering, Multimedia University, Persiaran Multimedia, Cyberjaya 63100, Malaysia
[4]Department of Electronics and Communication Engineering, Faculty of Engineering and Petroleum, Hadhramout University, Al-Mukalla 50512, Yemen
[5]Centre for Advanced Studies in Telecommunication (CAST), COMSATS University Islamabad (CUI), Islamabad 45550, Pakistan

Corresponding authors: Tayyab Shabbir (tayyab.shabbir@ukm.edu.my) and Mohammad Tariqul Islam (tariqul@ukm.edu.my)

This work was supported by the Universiti Kebangsaan Malaysia Research grant under Grant code MI-2019-015.

ABSTRACT In this article, an eight-element ultra-wideband (UWB) Multiple-Input-Multiple Output (MIMO) antenna system is proposed for 3D non-planar applications. The proposed UWB-MIMO antenna is installed around a polystyrene block in the 3D-octagonal arrangement. The eight radiating elements are placed on the sides of the octagonal polystyrene block with top and bottom surfaces left open. The single antenna element consists of a modified Y-shaped radiating patch, epsilon-negative (ENG) metamaterial, and a partial ground plane. A modified pie-shaped decoupling structure is deployed at the back-side of the radiating patch to improve the isolation among array elements. Each antenna element is printed on a low-cost FR-4 substrate with dimensions of 28 mm $\times$ 23 mm with coverage of the whole UWB spectrum from 3.1 to 10.6 GHz frequency band. The eight-port UWB-MIMO antenna system consists of symmetric and non-symmetric array configurations. Simulated and measured MIMO performance parameters i.e. Channel Capacity Loss (CCL) $<$ 0.35, Envelope Correlation Coefficient (ECC) $<$ 0.0025 and Total Active Reflection Coefficient (TARC) $<$ -11 dB are in acceptable limits for both symmetric and non-symmetric configurations. The proposed MIMO antenna system is suitable for 3D system-in-package, indoor localization systems, and wireless personal area network applications in industries where multiple machines are connected to a central server wirelessly through such kinds of antennas in a rich scattering environment.

INDEX TERMS Antenna, channel capacity loss (CCL), envelope correlation coefficient (ECC), metamaterial (MTM), multiple-input-multiple-output (MIMO), total active reflection coefficient (TARC), ultra-wideband (UWB).

I. INTRODUCTION

The microwave research community has put significant efforts in designing antennas in the ultra-wideband spectrum ever since the Federal Communications Commission (FCC) has announced its license free usage. However, the maximum allowable power spectral density in this band is -41dBm/MHz. This limitation has resulted in the reduction of both channel capacity and communication range for UWB technology [1]–[3]. A combination of UWB with MIMO technology has therefore emerged as an effective solution to overcome these limitations and has resulted in the evolution of several application areas. UWB-MIMO antenna systems usually consist of several radiating elements, placed in close proximity of one another, operate simultaneously to provide high diversity and multiplexing gain. In modern wireless communication miniaturized components are usually required [4]–[6] owing to space constraints and hence the closely placed antenna elements create significantly high mutual-coupling causing reduced performance.

The associate editor coordinating the review of this manuscript and approving it for publication was Walid Al-Hussaibi.

Mutual coupling reduction between antenna elements is a major challenge in the design of the UWB-MIMO antenna system. The individual antenna elements must be properly matched to the system impedance also and effectively decoupled from the adjacent MIMO elements [7], [8].

In the reported literature, several techniques have been employed to suppress the mutual coupling between array elements. These techniques include: Defected ground structures (DGS) [9]–[11], Frequency Selective Surfaces (FSSs) [12], stub loading [13], [14], neutralization lines [15], patterned grounds [16], metamaterial isolator [17], meander line resonator [18], and parasitic elements [19], etc. Existing literature mostly reports on planar topologies, however, a few non-planar configurations for the MIMO antenna system have also been reported in [4], [19], [20].

A two elements non-planar UWB-MIMO antenna system is presented in [19], having dimensions of 40 mm $\times$ 37.5 mm $\times$ 41.5 mm with the isolation of 20 dB for the complete UWB frequency band. Moreover, radiating elements in a square configuration are etched on a low-cost FR-4 substrate, high isolation is achieved by introducing vertical stubs and C- shaped strips on the rear-side of the substrate. In another study, four elements non-planar UWB-MIMO antenna system is discussed [4]. Frequency Selective Surface based decoupling structures offer isolation of more than 20 dB in most of the frequency band. This UWB-MIMO configuration with dimensions of 32 mm $\times$ 36 mm is proposed for 3D system-in-package applications. An eight-port non-planar diversity antenna with multiple polarizations is reported in [20]. A set of four antennas are placed horizontally while the rest of the antennas are arranged in the vertical direction. In [21], a dielectric resonator integrated eight-port MIMO system with pattern diversity is presented. This array configuration provides isolation of more than 20 dB, correlation level of 0.25, and TARC less than - 15 dB. A compact 3D UWB-MIMO antenna is discussed in [22]. Four antenna elements are placed in a planar configuration while the remaining four elements are placed in a non-planar configuration. Isolation of 20 dB along with ECC less than 0.5 is achieved in the complete UWB frequency band.

Several planar UWB-MIMO geometries are reported in the literature [23]–[27]. The eight-port planar UWB-MIMO antenna for polarization and pattern diversity is discussed in [23]. Isolation of more than 15 dB with envelop correlation coefficient less than 0.1 is achieved for all ports. In another study, an 8-port ultra-wideband antenna system for smartphone applications is reported in [24]. In this configuration, an isolation level of 15 dB and a correlation coefficient better than 0.1 is obtained for smartphone applications. The MIMO design proposed in [25] has two identical half-slot antenna elements with a Y-shaped cut in the ground plane. This compact MIMO antenna has an isolation of 15 dB in the lower frequency band. Whereas, mutual coupling suppression of more than 20 dB is achieved in the higher frequency band of UWB. Another planar MIMO system with an orthogonally dual-polarized antenna system is reported in [26]. This MIMO configuration has eight elements connected with square rings. This configuration provides isolation of 15 dB. Similarly, a two-element planar MIMO antenna system with band notch characteristics is discussed in [27]. This MIMO configuration has an isolation of 20 dB with more than 85% efficiency in the entire UWB band. The metamaterial (MTM) loaded UWB antenna system design is a novel approach to obtain a high gain, improved radiation performance, and large bandwidth with miniaturized antenna size [28], [29]. A compact printed monopole antenna integrated with a single negative metamaterial is proposed in [28]. This UWB antenna configuration has a compact size of 22.5 mm $\times$ 14 mm with a peak gain of 6.12 dBi and a radiation efficiency of more than 80%. In [30], a two-layer integrated metamaterial-based antenna system is discussed. The π-shape and cross-shaped slots are used to enhance the frequency band and radiation efficiency of the proposed antenna system.

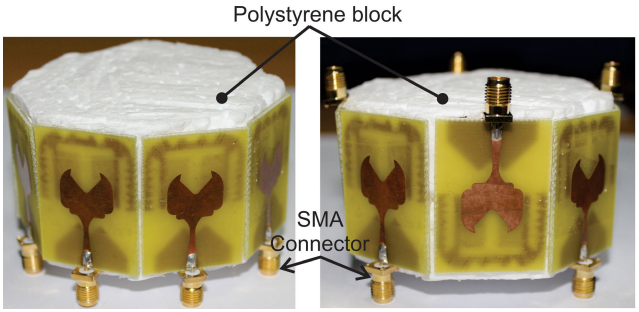

FIGURE 1. Fabricated eight-port UWB-MIMO prototype with symmetric and non-symmetric configurations.

In this article, an eight-element UWB-MIMO antenna system is presented with symmetric as well as non-symmetric configurations, as shown in Fig. 1. The antenna elements are placed in the 3D octagonal arrangement around a polystyrene block. Isolation of more than 20 dB and MIMO performance parameters (ECC, TARC, and CCL) in acceptable limits are achieved for both configurations. A commercially available full-wave 3D simulator, High Frequency Structural Simulator (HFSS), is used to design and analyze the eight-port UWB-MIMO system. The proposed 3D non-planar UWB-MIMO system is suitable for system-in-package applications and wireless personal area network applications in industries where multiple machines are connected to a central server wirelessly through these kinds of antennas in a rich scattering environment. The rest of the paper is structured as follows: Section II describes the metamaterial unit cell analysis. Single element UWB antenna design along with eight-port UWB-MIMO configuration is discussed in Section III. The simulated and measured results, along with the MIMO performance parameters are described in Section IV. Finally, the manuscript is concluded in Section V.

II. METAMATERIAL DESIGN AND ANALYSIS

The metamaterial (MTM) unit cell is designed and analyzed by using a Finite Element Method (FEM) provided in the sim-

ulator. The metamaterial unit cell is designed on a low-cost FR-4 substrate with a dielectric constant of 4.4, a thickness of 1.5 mm, and copper cladding of 0.035 mm. The proposed unit element consists of two square rings. Each ring contains two gaps introduced 1 mm away from the diagonally opposite corners. However, inner split-ring is attached with a meander-line structure by using two horizontal stubs. The metamaterial unit cell configuration, dimensions, and simulation setup are shown in Fig. 2.

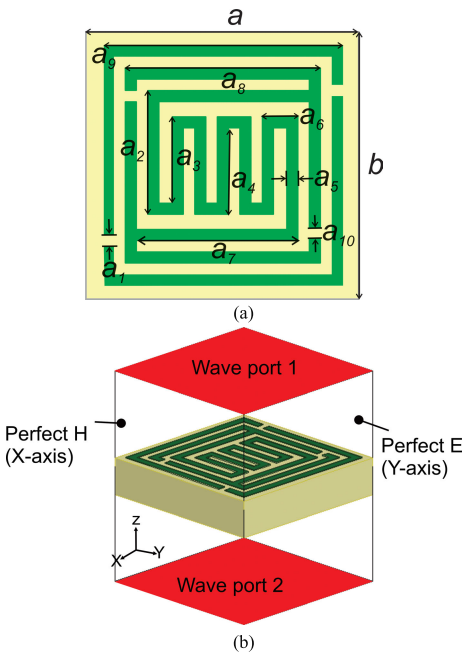

FIGURE 2. Metamaterial unit cell configuration and simulation setup (a). Unit cell configuration (b). Analysis setup.

The metamaterial unit cell was placed between two wave ports on the negative and positive z-axis and excited with an electromagnetic wave in the positive z-axis direction. To achieve negative characteristics, perfect magnetic boundary conditions have been set along the x-axis, and perfect electric boundaries are chosen for the y-axis [31]. The z-axis was chosen for free-space propagation of incoming waves as shown in Fig. 2b. The analysis of surface current distribution is carried out to understand the physical phenomena of Epsilon Negative (ENG) metamaterial structure. The surface current distribution at 3.9 GHz, 5.2 GHz, 7.5 GHz, and 10.15 GHz is plotted in Fig. 3. A large concentration of surface current can be observed at meander-line structure, inner rings gaps/splits, and corners. The current flows in opposite directions in the meander line structure and the split rings. This current direction reversal generates a stop band at 3.9 GHz, 5. GHz and 10.15 GHz frequency bands. Moreover, a strong current distribution at the inner ring, outer ring, and middle of the meander line structure create a wide stop-band response at 7.5 GHz frequency band. The splits/gaps in metamaterial structure act like capacitors and metallic rings act as inductors. The unit cell scattering parameters

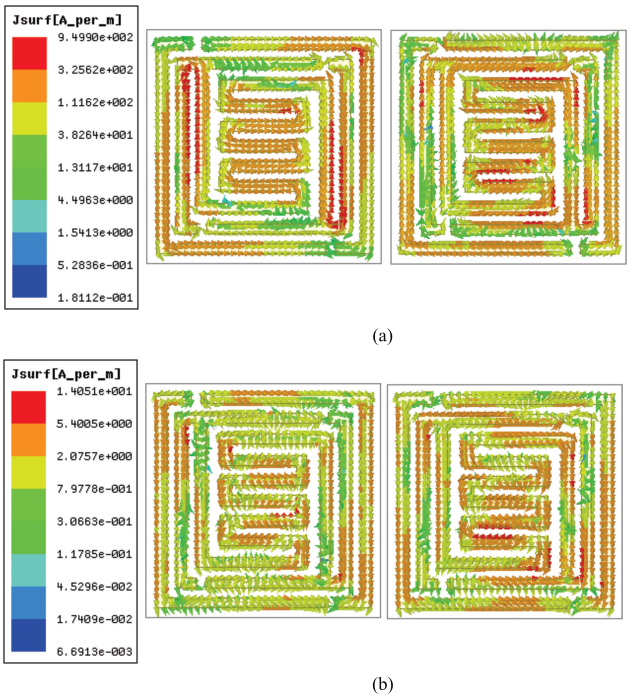

FIGURE 3. Metamaterial unit cell surface current distribution (a). 3.9 GHz (left) and 5.2 GHz (right) (b). 7.5 GHz (left) and 10.15 GHz (right).

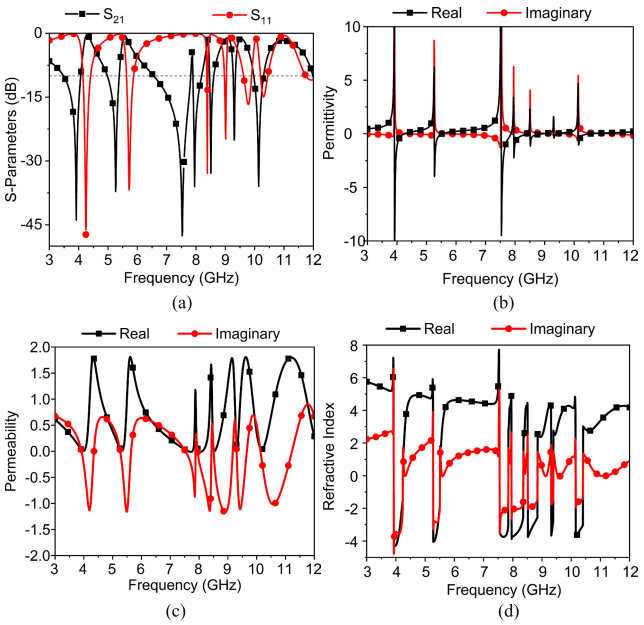

FIGURE 4. Metamaterial unit element simulation results (a). S-parameters (b). Permittivity (b). Permeability (c). Refractive index.

(S_{11} and S_{21}) are plotted in Fig. 4. It shows a stop-band in 3.48 – 4.06 GHz, 5 – 5.37 GHz, 6.5 – 7.82 GHz, 7.90 – 8.2 GHz, 8.45 – 8.61 GHz, 9.25 – 9.36 GHz, and 9.90 – 10.35 GHz frequency bands.

The outer and inner split ring resonators along with meander-line structure are enough to achieve an effective stop-band operation within the UWB frequency band. The metamaterial structure acts like an inductance-capacitance

(LC) resonator. The metallic rings along with meander-line structure act as inductors and the splits/gaps act as capacitors that can control the resonance characteristics of the unit element [32], [33]. The metamaterial unit cell optimized parameters are: a = 7 mm, b = 7 mm, a_1 = 0.24 mm, a_2 = 2.64 mm, a_3 = 1.84 mm, a_4 = 1.84 mm, a_5 = 0.23 mm, a_6 = 0.69 mm, a_7 = 3.3 mm, a_8 = 3.9 mm, a_9 = 6.40 mm and a_{10} = 0.24 mm. The metamaterial constitutive parameters (permittivity, permeability, and refractive index) for 2 – 12 GHz frequency band are extracted by using a robust method provided in [28], [34].

$$S_{11} = \frac{R_{01}\left(1 - e^{i2n\kappa_0 d}\right)}{\left(1 - R_{01}^2 e^{i2n\kappa_0 d}\right)} \tag{1}$$

$$S_{21} = \frac{\left(1 - e^{i2n\kappa_0 d}\right)}{\left(1 - R_{01}^2 e^{i2n\kappa_0 d}\right)} \tag{2}$$

$$R_{01} = \frac{(Z-1)}{(Z+1)} \tag{3}$$

$$\text{Real}\,(z) \geq 0 \tag{4}$$

$$\text{Imaginary}\,(n) \geq 0 \tag{5}$$

$$z = \pm\sqrt{\frac{(1+S_{11})^2 - S_{21}^2}{(1-S_{11})^2 - S_{21}^2}} \tag{6}$$

$$e^{i2n\kappa_0 d} = \frac{S_{21}}{1 - S_{11}\frac{Z-1}{Z+1}} \tag{7}$$

$$n = \frac{1}{k_0 d}\left\{\left[imaginary\left[\ln e^{ink_0 d}\right] + 2m\pi\right] - i\left[real\left[\ln e^{ink_0 d}\right]\right]\right\} \tag{8}$$

The permittivity and permeability can be extracted by using the following relations:

$$\varepsilon = \frac{n}{z} \tag{9}$$

$$\mu = nz \tag{10}$$

In Robust Method, equations (1) to (10) are used to retrieve the effective metamaterial characteristics. The metamaterial unit cell reflection and transmission parameters are used to extract the permittivity, permeability, and refractive index characteristics of the metamaterial structure. The real and imaginary parts of permittivity, permeability, and refractive index are shown in Fig. 4. The proposed metamaterial structure shows ENG metamaterial properties in frequency bands: 3.48 – 4.06 GHz, 5 – 5.37 GHz, 6.5 – 7.82 GHz, 7.90 – 8.2 GHz, 8.45 – 8.61 GHz, 9.25 – 9.36 GHz, and 9.90 – 10.35 GHz. In these frequency bands, MTM has negative permittivity and refractive index.

III. METAMATERIAL LOADED ULTRA-WIDEBAND ANTENNA AND EIGHT ELEMENTS ARRAY

The metamaterial loaded UWB antenna element is designed in the first stage. Secondly, eight-port UWB-MIMO, along with decoupling structure is designed for symmetric and non-symmetric configurations.

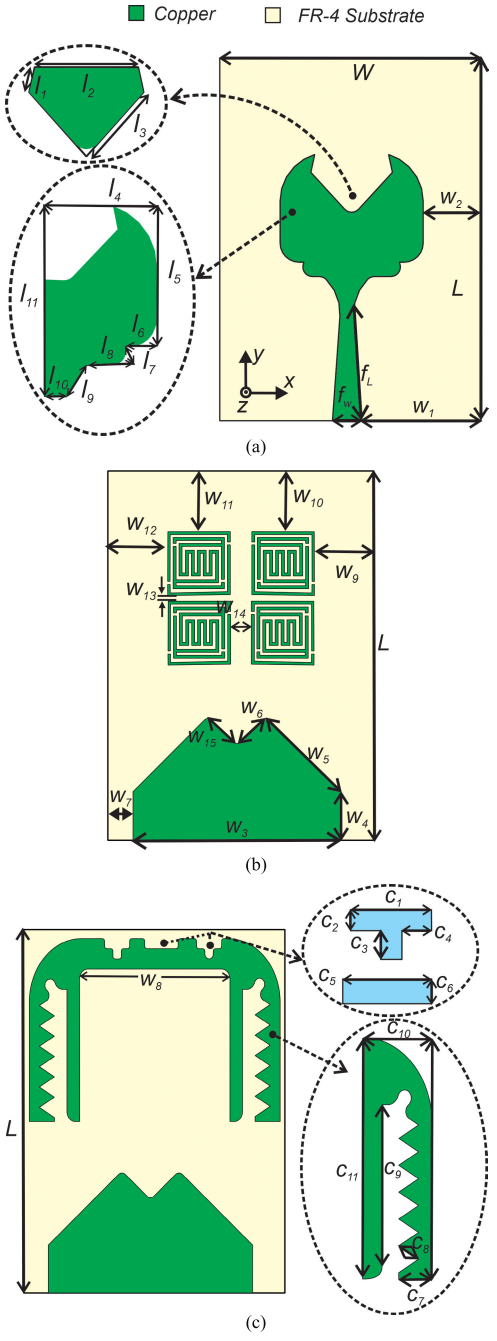

FIGURE 5. UWB antenna top and bottom layer with metamaterial and decoupling structure (a). Top layer radiating patch (b). Ground plane with ENG array (c). Decoupling structure at the rear-side of the radiating patch.

A. UNIT ELEMENT DESIGN AND ANALYSIS

The proposed UWB antenna geometry has been evolved from a rectangular microstrip patch. A low-cost 1.5 mm thick FR-4 substrate is used with relative permittivity of 4.4 and loss tangent of 0.02. A modified Y-shaped rectangular patch is chamfered from the top corners to improve the impedance matching over the whole band of interest. A beveled stepped structure is introduced at the lower edge of the patch, which is attached to a tapered feed-line. This stepped structure and the

TABLE 1. Eight-port UWB-MIMO array optimized parameters.

Parameters	L	W	f_L	f_W	W_1	W_2	W_3
value(mm)	28	23	8.7	2.3	10.5	5.6	15.3
Parameters	W_4	W_5	W_6	W_7	W_8	W_9	W_{10}
Value(mm)	4	8.2	2.90	3.83	10	3.5	3.55
Parameters	W_{11}	W_{12}	W_{13}	W_{14}	W_{15}	l_1	l_2
Value (mm)	3.55	3.5	1.2	2.5	2.90	1.53	5.9
Parameters	l_3	l_4	l_5	l_6	l_7	l_8	l_9
Value(mm)	4.15	4.8	7.5	1.5	2.46	1.35	1.4
Parameters	l_{10}	l_{11}	c_1	c_2	c_3	c_4	c_5
Value(mm)	0.56	12.5	1.84	0.64	0.64	0.61	2.4
Parameters	c_6	c_7	c_8	c_9	c_{10}	c_{11}	-
Value(mm)	0.64	1.84	1.27	7.7	3.7	9	

beveled region act as an impedance transformer. The feed-line width is linearly decreased from 2.3 mm to 0.8 mm. All edges in the radiating patch are beveled with a radius of 1 mm. The partial ground plane is applied at the rear-side along with tapered sides to achieve good impedance matching in the UWB frequency band. The UWB antenna front and back-side views are shown in Fig. 5. Moreover, UWB antenna optimized parameters are shown in Table 1.

The effect of different modifications is shown in Fig. 6(a). A simple microstrip patch shown in stage-A has a narrow bandwidth. A stepped response is introduced in stage-B to achieve a better impedance matching at the lower frequency band. The beveled feed-line along with truncated radiating patch and beveled corners, shown in stage C and D, provides better impedance matching for 3.1 – 10.6 GHz frequency band. The effect of ground plane size and shapes is shown in Fig. 6 (b). More stable response with impedance matching at the start band is achieved with a partial ground plane with chamfered sides. Moreover, 1 × 2 elements MTM array is placed at the back-side of the radiating patch to enhance the gain and efficiency of the UWB antenna. The MTM has ENG characteristics within 3.1 – 10.6 GHz frequency band.

The effect of MTM on the gain and efficiency of the UWB antenna is shown in Fig. 6(c). More than 60% enhancement in gain and efficiency is achieved by employing the metamaterial array at the backside of the radiating patch.

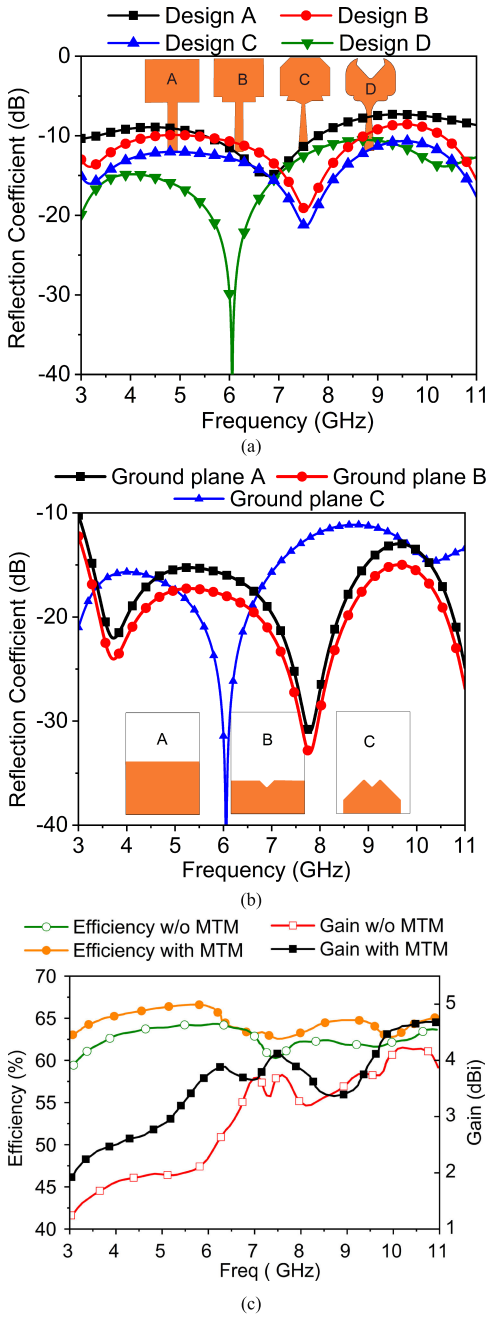

FIGURE 6. UWB antenna design methodology along with radiating patch and ground plane effect (a). Antenna radiating patch shape selection (b). Ground plane alteration effect (c). Gain and efficiency of UWB antenna with and without metamaterial (MTM) array.

B. EIGHT PORT UWB-MIMO AND DECOUPLING STRUCTURE DESIGN

The eight-port UWB-MIMO antenna system is intended to be used off devices at a convenient location to establish a strong communication link in rich scattered environments like hospital rooms or production lines. The UWB-MIMO antenna elements are installed around an octagonal shaped polystyrene block of permittivity 2.6. The octagonal shape has a radius of 33 mm; each face of the octagon has a width of 25 mm and a height of 32 mm. The eight antenna elements are installed on each face of the octagon resulting in a 45° angle between adjacent elements. Two adjacent elements have a pitch of 28.5 mm, while the distance between two opposite antenna elements is 60.52 mm as shown in Fig. 7.

The eight-port metamaterial loaded UWB-MIMO antenna system is arranged in two different configurations. In the first setup, referred to as symmetric configuration, all antenna ports are placed on the same side. Whereas in the non-symmetric configuration adjacent antennas have ports in the opposite directions. The UWB-MIMO antenna elements are categorized in edge-to-edge(E2E) and back-to-back(B2B)

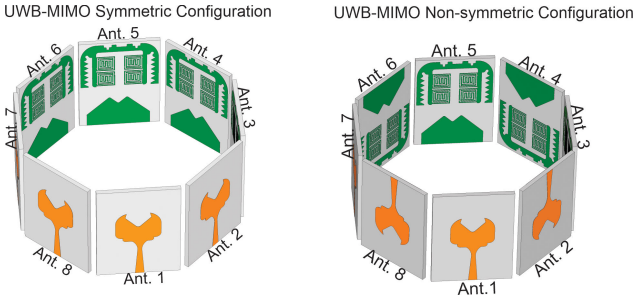

FIGURE 7. Eight port UWB-MIMO prototype with symmetric and non-symmetric configuration.

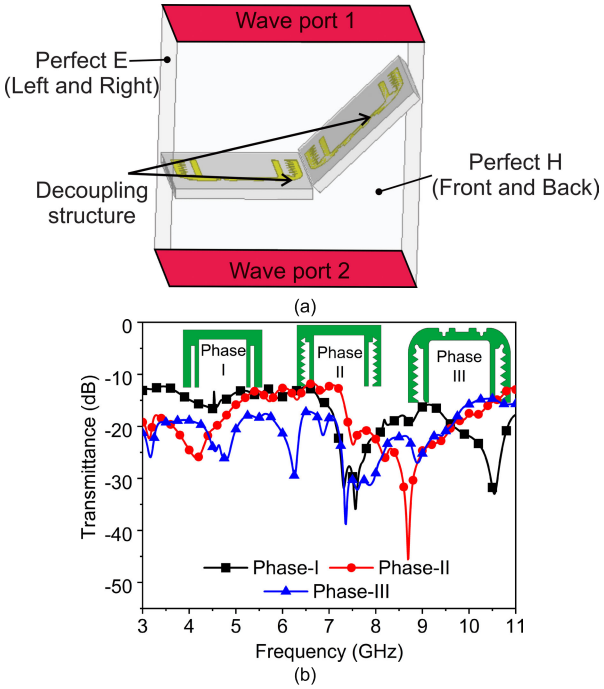

FIGURE 8. Decoupling structure design methodology and analysis for edge-to-edge elements (Ant. 1 and Ant. 2) (a). Analysis setup (b). Transmission loss.

arrangement for the sake of simplicity. The antenna elements (1, 5),(2, 6),(3, 7) and (4, 8) are in back-to-back (B2B) configuration relative to each other. Whereas, antenna elements (1, 2), (1, 3), and (1, 4) are in edge-to-edge (E2E) configuration in both symmetric and non-symmetric topology. These UWB-MIMO topologies require a very effective decoupling structure since the UWB antenna elements radiate in all directions thus developing a very strong mutual coupling.

A π shaped decoupling structure is designed and optimized for the proposed setup. This structure consists of four vertical stubs, the outer two stubs have zigzag edges while the inner stubs have plane edges. The decoupling structure analysis is performed by using wave ports, perfect electric, and magnetic boundary conditions configured in the simulator. The transmission loss variation with the decoupling structure modifications is shown in Fig. 8. PEC boundary conditions are assigned to the left and right side of the airbox. In contrast,

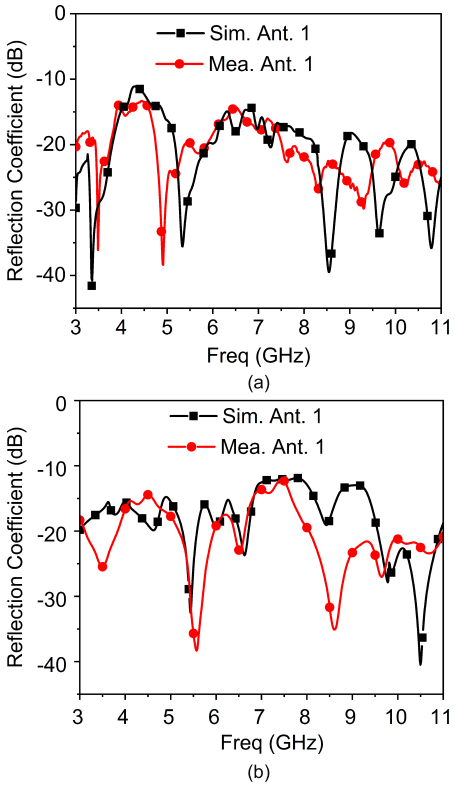

FIGURE 9. Simulated and measured reflection coefficient of eight-port UWB-MIMO antenna (a). Symmetric configuration (b). Non-symmetric configuration.

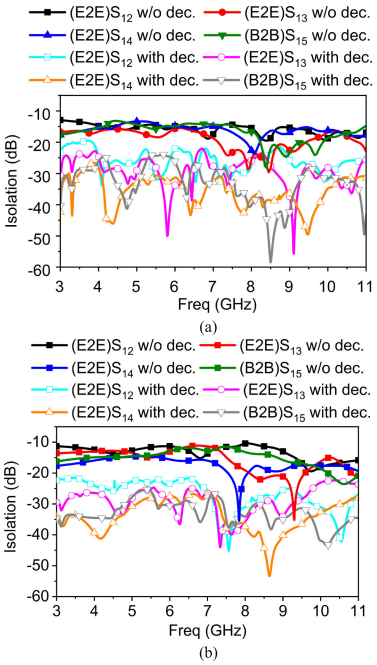

FIGURE 10. Mutual coupling with and without decoupling structure for B2B and E2E elements (a). Symmetric configuration (b). Non-symmetric configuration.

PMC boundaries are applied to the front and backside of the radiation box. The decoupling structure is excited by employing wave ports on the top and bottom face of the airbox.

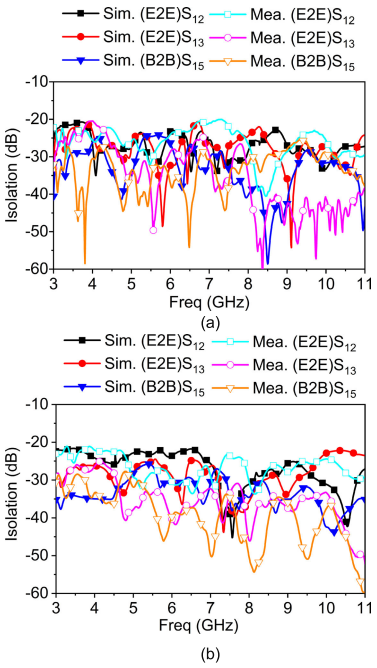

FIGURE 11. Simulated and measured isolation/decoupling performance of UWB-MIMO configuration (a). Symmetric configuration (b). Non-symmetric configurations.

The four vertical stubs along with slotted middle stub and zigzag pattern in outer stub are used to reduce the mutual coupling between antennas in B2B and E2E configurations.

The final optimized decoupling structure has evolved in three iterations as shown in Fig. 8. The final evolution step involves the introduction of several defects in order to achieve the desired decoupling level for the whole UWB frequency spectrum for both symmetric and non-symmetric arrangements.

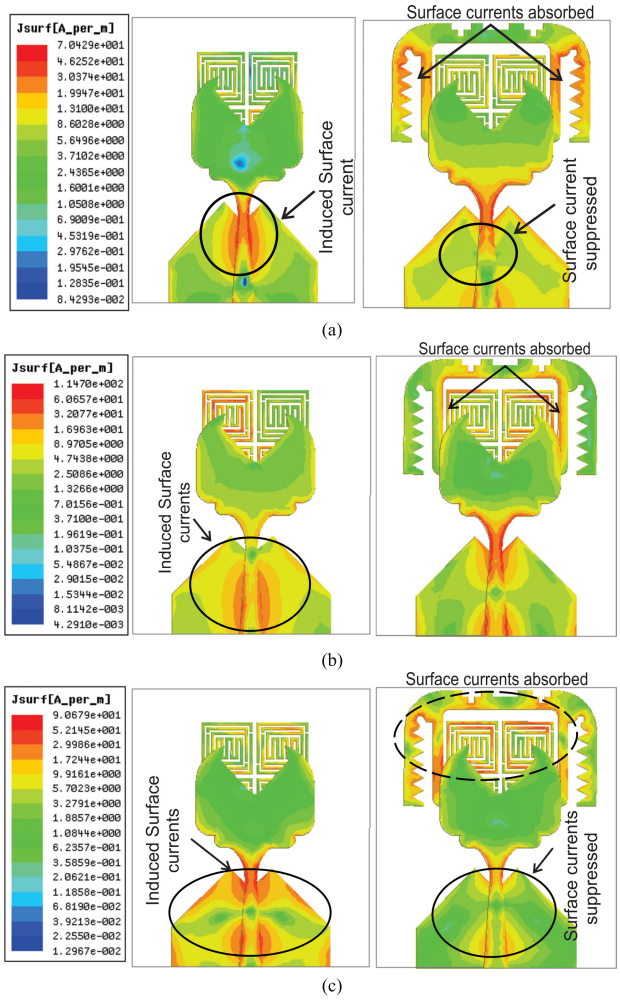

FIGURE 12. Surface current distribution (a). 4 GHz (b). 7 GHz (c). 10 GHz.

IV. RESULTS AND DISCUSSION

The proposed MIMO system is intended for UWB applications. Therefore, wideband impedance matching is imperative. The matching over the whole frequency band is achieved by different modifications which involve the variation of antenna geometry as well as the ground plane and introduction of an ENG metamaterial structure. The simulated and measured reflection coefficient of the symmetric and non-symmetric UWB-MIMO antenna system is presented in Fig. 9. Eight identical UWB antenna elements are used for MIMO synthesis in a non-planar arrangement around an octagonal polystyrene block, as shown in Fig. 7. Therefore, all antenna elements have the same simulated and measured reflection coefficient. The reflection coefficient for an antenna is less than -10 dB in the whole UWB frequency band irrespective of its configuration.

The mutual coupling effect with and without decoupling structure is illustrated in Fig. 10. Without decoupling structure a high mutual coupling is present between array elements. Moreover, the mutual coupling is significantly large among the adjacent elements. The decoupling structure helps to reduce the mutual coupling among array elements. Simulated and measured decoupling performance of the antenna system for both symmetric and non-symmetric configuration is shown in Fig. 11. The isolation for B2B and E2E antenna pairs in the entire UWB is better than 20 dB for symmetric and non-symmetric configurations. Moreover, the addition of polystyrene block does not affect the isolation.

However, losses in the polystyrene block increase the measured isolation at higher frequencies by impeding the coupled fields. It is observed that measured results have slightly deviated from simulations. The polystyrene used in the simulator was lossless. Therefore, an additional polystyrene effect on the reflection coefficient and isolation is not visible in simulated results. The polystyrene block is used as supporting material to hold the antenna elements. Moreover, 3D assembly imperfections during non-planar array formation and array elements placement contribute to these variations. Overall, polystyrene helps in the non-planar 3D arrangement of the MIMO system with no significant contribution to the results.

The surface currents distribution of the proposed UWB-MIMO antenna system at 4 GHz, 7 GHz, and 10 GHz are shown in Fig. 12. In the absence of a decoupling structure,

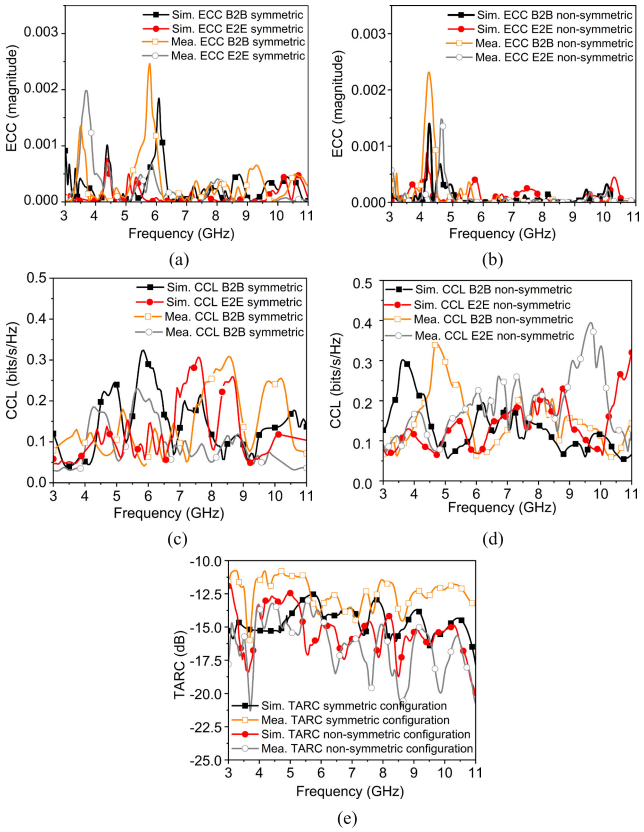

FIGURE 13. UWB-MIMO performance parameters (a). ECC symmetric configuration (b). ECC non-symmetric configuration (c). CCL symmetric configuration (d). CCL non-symmetric configuration (e). TARC.

TABLE 2. Comparison with recent UWB-MIMO antennas.

Ref. no	Geometry (element size) mm^3	Ports	Substrate	Isolation (dB)	TARC (dB)	ECC	CCL
[4]	Non-planar (32×36×1.5)	4	FR-4	20	-8	<0.0025	<0.2
[19]	Non-planar (40×37.5×1.5)	2	FR-4	20	-4	<0.1	0.5
[22]	Non-Planar (25×25×1.5)	8	Rogers TMM4	20	-	<0.05	-
[23]	Planar (29×17×0.8)	8	FR-4	15	-8	<0.1	-
[26]	Non-Planar -	8	FR-4	19	-	<0.12	-
[36]	Planar -	8	FR-4	11.2	-	<0.08	-
[37]	Planar (39×39×1.6)	4	FR-4	22	-10	<0.02	<0.2
This work	**Non-planar (23×28×1.5)**	**8**	FR-4	**20**	**-11**	**<0.0025**	**<0.35**

a strong induced current is observed. However, metamaterial structure and discontinuities in the decoupling structure in the shape of slots and zigzag patterns capture the electromagnetic field and convert them in induced currents. A significant

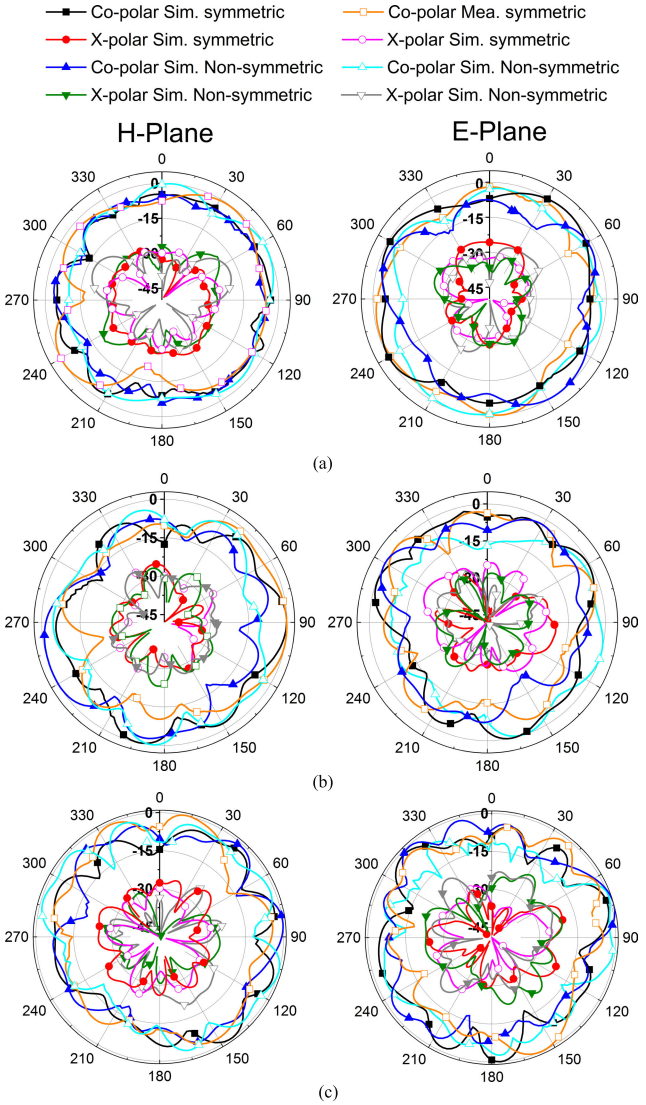

FIGURE 14. Simulated and measured radiation patterns for symmetric and non-symmetric configurations (a). 3 GHZ (b). 6 GHz (c). 10 GHz.

reduction is thus visible at lower, middle, and higher frequency bands.

The diversity performance of the metamaterial loaded UWB-MIMO antenna system in both configurations (symmetric and non-symmetric) is evaluated by the Envelope Correlation Coefficient (ECC), Channel Capacity Loss (CCL), and Total Active Reflection Coefficient (TARC). For an efficient UWB-MIMO system ECC, CCL and TARC should be below 0.5, 0.5 bits/s/Hz and 0 dB respectively [4]. The value of ECC is calculated from S-parameters with the help of the relation provided in [4], [19] which applies to a rich scattering environment that is under investigation in this research work.

The CCL of the proposed UWB-MIMO system is calculated for both symmetric and non-symmetric configurations. Moreover, ECC and CCL are calculated individually for both the E2E and B2B arrangements for the UWB-MIMO antenna system, whereas TARC is calculated for all of the eight

radiating antennas collectively. The simulated and measured ECC, CCL, and TARC of the proposed UWB-MIMO configuration are shown in Fig. 13. The simulated and measured values of performance parameters are within the desired limits.

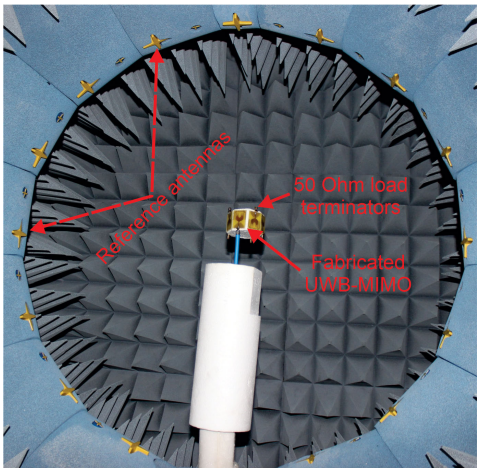

FIGURE 15. Eight-port metamaterial loaded UWB-MIMO antenna system in Satimo measurement setup.

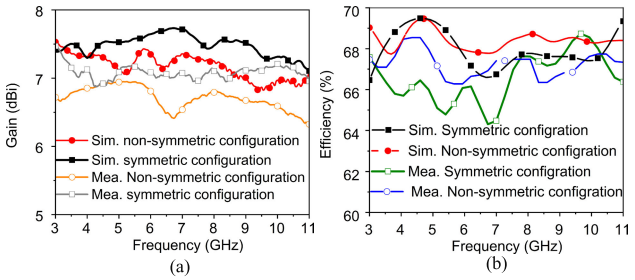

FIGURE 16. Far-field radiation performance of proposed eight-port UWB-MIMO antenna system (a). Gain (b). Efficiency.

The fabricated eight-port UWB-MIMO has been measured in Satimo near Field Measurement Lab by using Satimo Passive Measurement (SPM), SatEnv software, and Agilent N5227A vector network analyzer [35]. Simulated and measured radiation patterns for E-plane and H-plane at 4 GHz, 7 GHz, and 10 GHz are shown in Fig. 14. The antenna radiation patterns have shown some variations due to 3D assembly imperfection and measurement setup constraints. The UWB-MIMO measurement setup is shown in Fig. 15. The proposed metamaterial loaded UWB-MIMO system provides a maximum measured gain of 7 dBi along with an efficiency of more than 60% as shown in Fig. 16.

A comparison of the proposed UWB-MIMO design with the existing literature is given in Table 2. It can be noted that the proposed non-planar metamaterial loaded UWB-MIMO system competes very well with planar and non-planar designs. The size of the proposed UWB antenna is highly miniaturized in MIMO configuration, which is extremely difficult to achieve without sacrificing other performance parameters. Moreover, an isolation of 20 dB is achieved with TARC < -8 dB, ECC < 0.0025, CCL < 0.35, which is highly competitive to other proposed UWB-MIMO designs in both planar and non-planar configuration.

V. CONCLUSION

In this study, an eight-port UWB MIMO antenna system is presented. The proposed MIMO system is suitable for applications that require compact size and 3D non-planar arrangement. The customized design of patch antenna along with tapered feedline and ENG metamaterial ensure the impedance matching over the whole UWB spectrum. The mutual coupling reduction among antenna elements is achieved by introducing parasitic decoupling structure at antenna rear-sides. The metamaterial loaded MIMO system achieves isolation of 20 dB in the whole band. The significance of the proposed system is further established by MIMO performance parameters. The measured and simulated results are in good agreement. Eight-element planar arrangements require more space and cannot exploit spatial diversity as much as this scheme can do. The off-device installation of the antenna module is very helpful by conveniently placing it where the best reception is achieved.

REFERENCES

[1] D. Guha and Y. M. M. Antar, "Printed UWB antennas," in *Microstrip and Printed Antennas: New Trends, Techniques and Applications*. Hoboken, NJ, USA: Wiley, 2011, pp. 305–343.
[2] M. A. W. Nordin, M. T. Islam, and N. Misran, "Design of a Compact Ultrawideband Metamaterial Antenna Based on the Modified Split-Ring Resonator and Capacitively Loaded Strips Unit Cell," *Prog. Electromagn. Res.*, vol. 136, pp. 157–173, 2013.
[3] R. Azim, M. T. Islam, and N. Misran, "A planar monopole antenna for UWB applications," *Int. Rev. Electr. Eng.*, vol. 10, no. 4, pp. 1848–1852, 2010.
[4] M. Bilal, R. Saleem, H. H. Abbasi, M. F. Shafique, and A. K. Brown, "An FSS-based nonplanar quad-element UWB-MIMO antenna system," *IEEE Antennas Wireless Propag. Lett.*, vol. 16, pp. 987–990, 2017.
[5] H. AL-Saif, M. Usman, M. T. Chughtai, and J. Nasir, "Compact ultra-wide band MIMO antenna system for lower 5G bands," *Wireless Commun. Mobile Comput.*, vol. 2018, pp. 1–6, Jun. 2018.
[6] Q. D. Nguyen, T. T. Le, D. T. Le, X. N. Tran, and Y. Yamada, "A compact MIMO ultra-wide band antenna with low mutual coupling," *Appl. Comput. Electromagn. Soc. J.*, vol. 31, no. 3, pp. 252–260, 2016.
[7] A. Mousazadeh and G. Dadashzadeh, "A novel compact UWB monopole antenna with triple band-notched characteristics with EBG structure and two folded V-slot for MIMO/diversity applications," *Appl. Comput. Electromagn. Soc. J.*, vol. 31, no. 1, pp. 1–7, 2016.
[8] T. Shabbir, R. Saleem, A. Akram, and M. F. Shafique, "UWB-MIMO quadruple with FSS-inspired decoupling structures and defected grounds," *Appl. Comput. Electromagn. Soc. J.*, vol. 30, no. 2, pp. 184–190, 2015.
[9] M. A. Ul Haq and S. Koziel, "Ground plane alterations for design of high-isolation compact wideband MIMO antenna," *IEEE Access*, vol. 6, pp. 48978–48983, 2018.
[10] A. Ghalib and M. S. Sharawi, "TCM analysis of defected ground structures for MIMO antenna designs in mobile terminals," *IEEE Access*, vol. 5, pp. 19680–19692, 2017.
[11] K. Wei, L. Wang, Z. Xing, R. Xu, and J. Li, "S-shaped periodic defected ground structures to reduce microstrip antenna array mutual coupling," *Electron. Lett.*, vol. 52, no. 15, pp. 1288–1290, Jul. 2016.
[12] T. Hassan, M. U. Khan, H. Attia, and M. S. Sharawi, "An FSS based correlation reduction technique for MIMO antennas," *IEEE Trans. Antennas Propag.*, vol. 66, no. 9, pp. 4900–4905, Sep. 2018.
[13] A. Iqbal, O. A. Saraereh, A. W. Ahmad, and S. Bashir, "Mutual coupling reduction using F-shaped stubs in UWB-MIMO antenna," *IEEE Access*, vol. 6, pp. 2755–2759, 2018.

[14] Y. Yin, J. Hong, C. Luo, and M. Amin, "A compact planar UWB MIMO antenna using modified ground stub structure," *IEICE Electron. Exp.*, vol. 14, no. 20, p. 20170883, Sep. 2017.
[15] S. Zhang and G. F. Pedersen, "Mutual coupling reduction for UWB MIMO antennas with a wideband neutralization line," *IEEE Antennas Wireless Propag. Lett.*, vol. 15, pp. 166–169, 2016.
[16] D. Wu, S. W. Cheung, Q. L. Li, and T. I. Yuk, "Decoupling using diamond-shaped patterned ground resonator for small MIMO antennas," *IET Microw., Antennas Propag.*, vol. 11, no. 2, pp. 177–183, Jan. 2017.
[17] F. Wang, Z. Duan, S. Li, Z.-L. Wang, and Y.-B. Gong, "Compact UWB MIMO Antenna with Metamaterial-Inspired Isolator," *Prog. Electromagn. Res. C*, vol. 84, pp. 61–74, 2018.
[18] J. Ghosh, S. Ghosal, D. Mitra, and S. R. B. Chaudhuri, "Mutual coupling reduction between closely placed microstrip patch antenna using meander line resonator," *Prog. Electromagn. Res. Lett.*, vol. 59, pp. 115–122, 2016.
[19] S. I. Jafri, A. K. Brown, M. F. Shafique, and R. Saleem, "Compact reconfigurable multiple-input-multiple-output antenna for ultra wideband applications," *IET Microw., Antennas Propag.*, vol. 10, no. 4, pp. 413–419, Mar. 2016.
[20] S. K. Palaniswamy, Y. P. Selvam, M. G. N. Alsath, M. Kanagasabai, S. Kingsly, and S. Subbaraj, "3-D eight-port ultrawideband antenna array for diversity applications," *IEEE Antennas Wireless Propag. Lett.*, vol. 16, pp. 569–572, 2017.
[21] G. Das, N. K. Sahu, A. Sharma, R. K. Gangwar, and M. S. Sharawi, "Dielectric resonator-based four-element eight-port MIMO antenna with multi-directional pattern diversity," *IET Microw., Antennas Propag.*, vol. 13, no. 1, pp. 16–22, Jan. 2019.
[22] M. S. Khan, F. Rigobello, B. Ijaz, E. Autizi, A. D. Capobianco, R. Shubair, and S. A. Khan, "Compact 3-D eight elements UWB-MIMO array," *Microw. Opt. Technol. Lett.*, vol. 60, no. 8, pp. 1967–1971, Aug. 2018.
[23] R. Mathur and S. Dwari, "8-port multibeam planar UWB-MIMO antenna with pattern and polarisation diversity," *IET Microw., Antennas Propag.*, vol. 13, no. 13, pp. 2297–2302, Oct. 2019.
[24] X. Zhang, Y. Li, W. Wang, and W. Shen, "Ultra-wideband 8-port MIMO antenna array for 5G metal-frame smartphones," *IEEE Access*, vol. 7, pp. 72273–72282, 2019.
[25] R. Mathur and S. Dwari, "Compact 4-port MIMO/diversity antenna with low correlation for UWB application," *Frequenz*, vol. 72, nos. 9–10, pp. 429–435, Aug. 2018.
[26] M.-Y. Li, Z.-Q. Xu, Y.-L. Ban, C.-Y.-D. Sim, and Z.-F. Yu, "Eight-port orthogonally dual-polarised MIMO antennas using loop structures for 5G smartphone," *IET Microw., Antennas Propag.*, vol. 11, no. 12, pp. 1810–1816, Sep. 2017.
[27] D. Yadav, M. P. Abegaonkar, S. K. Koul, V. N. Tiwari, and D. Bhatnagar, "Two element band-notched UWB MIMO antenna with high and uniform Isolation," *Prog. Electromagn. Res. M*, vol. 63, pp. 119–129, 2018.
[28] S. S. Al-Bawri, H. Hwang Goh, M. S. Islam, H. Y. Wong, M. F. Jamlos, A. Narbudowicz, M. Jusoh, T. Sabapathy, R. Khan, and M. T. Islam, "Compact ultra-wideband monopole antenna loaded with metamaterial," *Sensors*, vol. 20, no. 3, p. 796, Jan. 2020.
[29] F. H. Lin and Z. N. Chen, "A method of suppressing higher order modes for improving radiation performance of metasurface multiport antennas using characteristic mode analysis," *IEEE Trans. Antennas Propag.*, vol. 66, no. 4, pp. 1894–1902, Apr. 2018.
[30] G. K. Pandey, H. S. Singh, M. K. Meshram, and P. K. Bharti, "Metamaterial-based UWB antenna," *Electron. Lett.*, vol. 50, no. 18, pp. 1266–1268, Aug. 2014.
[31] M. Ullah, M. Islam, and M. Faruque, "A near-zero refractive index meta-surface structure for antenna performance improvement," *Materials*, vol. 6, no. 11, pp. 5058–5068, Nov. 2013.
[32] S. S. Islam, M. R. I. Faruque, and M. T. Islam, "A near zero refractive index metamaterial for electromagnetic invisibility cloaking operation," *Materials*, vol. 8, no. 8, pp. 5058–5068, 2013.
[33] S. S. Islam, M. R. I. Faruque, and M. T. Islam, "A new direct retrieval method of refractive index for the metamaterial," *Current Sci.*, vol. 109, no. 2, pp. 337–342, 2015.
[34] A. B. Numan and M. S. Sharawi, "Extraction of material parameters for metamaterials using a full-wave simulator [education column]," *IEEE Antennas Propag. Mag.*, vol. 55, no. 5, pp. 202–211, Oct. 2013.
[35] A. Salleh, C. C. Yang, T. Alam, M. S. J. Singh, M. Samsuzzaman, and M. T. Islam, "Development of microwave brain stroke imaging system using multiple antipodal Vivaldi antennas based on raspberry Pi technology," *Jurnal Kejuruteraan (J. Eng.)*, vol. 32, no. 1, pp. 39–49, 2020.
[36] J. Li, X. Zhang, Z. Wang, X. Chen, J. Chen, Y. Li, and A. Zhang, "Dual-band eight-antenna array design for MIMO applications in 5G mobile terminals," *IEEE Access*, vol. 7, pp. 71636–71644, 2019.
[37] Z. Tang, X. Wu, J. Zhan, S. Hu, Z. Xi, and Y. Liu, "Compact UWB-MIMO antenna with high isolation and triple band-notched characteristics," *IEEE Access*, vol. 7, pp. 19856–19865, 2019.

TAYYAB SHABBIR received the B.S. degree in electrical (telecommunication) engineering from the COMSATS Institute of Information Technology (CIIT), Islamabad, Pakistan, in 2011, and the master's degree in telecommunication engineering and the Ph.D. degree in antennas and electromagnetics from the University of Engineering and Technology (UET), Taxila, Pakistan, in 2014 and 2019, respectively. He is currently working as a Postdoctoral Researcher with the Department of Electrical, Electronic and Systems Engineering, Universiti Kebangsaan Malaysia (UKM), Malaysia. He has published papers in many reputable scientific journals and conferences. His current research interests include UWB-MIMO systems, metamaterials, high gain portable devices, frequency selective surfaces, and reflectarrays. He was a recipient of fully funded scholarship for his master's and Ph.D. degrees.

RASHID SALEEM received the B.S. degree in electronic engineering from the Ghulam Ishaq Khan Institute of Engineering Sciences and Technology, Pakistan, in 1999, the M.S. degree from the UET Taxila through Center for Advanced Studies in Engineering, Pakistan, in 2006, and the Ph.D. degree from The University of Manchester, U.K., in 2011. He pursued a Career in the telecommunication industry for several years while continuing education. In his Ph.D., he worked in Microwave and Communication Systems research group under the supervision of Prof. A. K. Brown, the Head of the School of Electrical and Electronic Engineering, The University of Manchester. He worked on antennas, channel modeling and interference aspects of Ultra-Wideband systems during his Ph.D. and was also a member of a team designing and testing arrays for the Square Kilometer Array project. He is currently working as an Tenured Associate Professor with the University of Engineering and Technology (UET), Taxila, Pakistan, where he is supervising several postgraduate students and heading the MAP (Microwaves, Antennas and Propagation) research group. His research interests include antennas, angle-of-arrival based channel modeling, microwave periodic structures, and metamaterials.

SAMIR SALEM AL-BAWRI (Member, IEEE) received the Master of Science degree in wireless communication engineering from Yarmouk University, Jordan, in 2009, and the Doctor of Philosophy degree in communication engineering from Universiti Malaysia Perlis (UniMAP), Malaysia, in 2018. He has served as a Lecturer at the Faculty of Engineering and Petroleum, Hadhramout University (HU), Yemen, from December 2009 to August 2014. He has served as a Graduate Research Assistance with UniMAP, from 2015 to 2018. He is currently an Assistant Professor with HU. He is also working as a Postdoctoral Researcher Fellow with Multimedia University - MMU, Malaysia. He has authored or coauthored over (10) ISI and SCOPUS published journal; (19) conference proceeding and working currently toward the 1st patent. His research interests include digital signal processing, design and evaluation of multi-element antennas, metamaterials, localization estimation techniques, and wireless propagation. He was a recipient of the Gold Medal Award at the Breakthrough Invention, Innovation and Design Exhibition Biide 2019 - UiTM.

MUHAMMAD FARHAN SHAFIQUE (Senior Member, IEEE) received the B.Eng. degree from Hamdard University, Karachi, Pakistan, in 2003, the M.S. degree from the University of Paris East Marne-La-Vallee, Paris, France, in 2005, and the Ph.D. degree in electronic and communications engineering from the University of Leeds, Leeds, U.K., in 2010. From 2007 to 2010, he was involved in establishing the LTCC fabrication facility with the Institute of Microwave and Photonics, the University of Leeds. He has extensive experience of laser micromachining and multilayer LTCC device modeling and fabrication. He is currently an Associate Professor with COMSATS University Islamabad (CUI), Pakistan. He is also a Founder Head of the MCAD Research Group, the Associate Director of the Center for Advanced Studies in telecommunications. He is also involved in dielectric characterization of materials using microwave techniques and fabrication of ceramic microfluidic devices. His research interests include multilayered-microwave device fabrication on LTCC and thick-film technology, RF antenna and antenna arrays, ultra-wideband diversity antennas, and MEMS packaging.

MOHAMMAD TARIQUL ISLAM (Senior Member, IEEE) is currently a Professor with the Department of Electrical, Electronic and Systems Engineering, Universiti Kebangsaan Malaysia (UKM) and a Visiting Professor with the Kyushu Institute of Technology, Japan. He is the author and coauthor of about 500 research journal articles, nearly 175 conference articles, and a few book chapters on various topics related to antennas, microwaves, and electromagnetic radiation analysis with 20 inventory patents filed. Thus far, his publications have been cited 5641 times and his H-index is 38 (Source: Scopus). His Google scholar citation is 8200 and H-index is 42. He was a recipient of more than 40 research grants from the Malaysian Ministry of Science, Technology and Innovation, Ministry of Education, UKM research grant, international research grants from Japan and Saudi Arabia. His research interests include communication antenna design, satellite antennas, and electromagnetic radiation analysis. Dr. Islam has been serving as an Executive Committee member for IEEE AP/MTT/EMC Malaysia Chapter, since 2018, the Chartered Professional Engineer (CEng), a member of IET, U.K., and a Senior Member of IEICE, Japan. He received several International Gold Medal awards, a Best Invention in Telecommunication Award for his research and innovation, and best researcher awards at UKM, in 2010 and 2011. He was a recipient of 2018 and 2019 IEEE AP/MTT/EMC Malaysia Chapter, Excellent Award. He also won the best innovation award, in 2011, and the Best Research Group in ICT niche by UKM, in 2014. He was a recipient of Publication Award from Malaysian Space Agency, in 2014, 2013, 2010, and 2009, and the Best Paper Presentation Award, in 2012, International Symposium on Antennas and Propagation (ISAP 2012) at Nagoya, Japan, and in 2015 in IconSpace. He was an Associate Editor of *IET Electronics Letter*. He also serves as the Guest Editor, *Sensors* journal, and an Associate Editor for IEEE Access.